Soil Dynamics and Earthquake Engineering 31 (2011) 1678–1689

Contents lists available at ScienceDirect

Soil Dynamics and Earthquake Engineering

journal homepage: www.elsevier.com/locate/soildyn

Seismic failure modeling of concrete dams considering heterogeneity of concrete

Hong Zhong*, Gao Lin, Xiaoyan Li, Jianbo Li

Faculty of Infrastructure Engineering, Dalian University of Technology, Dalian 116024, China

ARTICLE INFO

Article history:
Received 25 September 2010
Received in revised form
29 June 2011
Accepted 5 July 2011

ABSTRACT

Study on the failure process of high concrete dams subjected to strong earthquakes is crucial to reasonable evaluation of their seismic safety. Numerical simulation in this aspect involves dynamic failure analysis of big bulk concrete dam subjected to cyclic loading. The Rock Failure Process Analysis (RFPA) proposed by C.A. Tang, with successful applications to failure modeling of rock and concrete specimens mainly subjected to static loading, is extended for this purpose. For using the proposed model, no knowledge on the cracking route needs to be known beforehand, and no remeshing is required. Simulation of the whole process of elastic deformation, initiation and propagation of microcracks, severe damage and ultimate failure of concrete dams in earthquakes with a unified model is enabled. The model is verified through a shaking table test of an arch dam. Finally a practical gravity dam is employed as a numerical example. Considering the uncertainty in ground motion input and concrete material, typical failure process and failure modes of gravity dam are presented. Several small cracks may occur due to tension particularly at dam neck, dam faces and dam heel, and a few of them evolve into dominant ones. Relatively smaller earthquake may cause damage to the dam neck while a bigger one may bring on cracks at lower parts of the dams. Cracking at the dam bottom may incline to a direction almost perpendicular to the downstream face after propagating horizontally for a certain distance when the shaking is strong enough.

© 2011 Elsevier Ltd. All rights reserved.

1. Introduction

With the outburst of strong earthquakes in China, Haiti and Chile during the last two years, it seems that the earth has come into an era with more and stronger earthquakes. The majority of high dams are being built or to be built in countries with active seismic activities such as China, Turkey, etc. Considering the possible disastrous results brought about by dam failures, seismic safety of high dams remains a crucial problem to be solved in dam construction. In the seismic design guidelines in China [1], two levels of earthquakes are adopted. The design of earthquake is assumed with non-exceeding probability of 98% in one hundred years, and 99% of non-exceeding probability is assumed for the checking of earthquake. However, Shapai Arch Dam, with a design PGA of 0.10 g, has undergone earthquake shocks with an intensity higher than IX in the Wenchuan Earthquake in 2008 [2], which poses the problem that dams might be subjected to earthquake shocks much stronger than the design value owing to the complexity and randomness of seismic activities. Seismic analysis of concrete dams considering its failure process and failure modes, leading to more realistic and comprehensive insights into the seismic response of dams, has become one important frontier in dam analysis.

Seismic hazard documents and shaking table tests are our main sources of understanding the seismic failure of high concrete dams. However, there are only few examples of high concrete dams subjected to strong earthquakes shocks, and cases of severe damage are even rare. The Xinfengjiang Dam, Sefid Rud Dam and Koyna Dam are the ones that have suffered damage in earthquakes. The shaking table test can reproduce the seismic response of any dams to dynamic loading, and models of many important dams have been shaken on the table to comprehensively investigate their seismic capacity [3,4]. For model tests, many issues need to be clarified. Among them, similarity relation is the most difficult particularly for a nonlinear response of the dam.

Numerical analysis is a promising alternative owing to the ability to take many factors into consideration and perform analysis of different cases with low costs. Many numerical models have been developed for the seismic nonlinear analysis of concrete dams. Among them, models in the context of Finite Element Method have gained the most popularity owing to the convenience in dealing with nonlinearity of concrete and complex geometry of structures. The discrete Crack Model (DCM) [5] and the Smeared Crack Model (SCM) [6] in the framework of Fracture Mechanics as well as

* Corresponding author. Tel./fax: +86 411 84709552.
E-mail address: hzhong@dlut.edu.cn (H. Zhong).

0267-7261/$ - see front matter © 2011 Elsevier Ltd. All rights reserved.
doi:10.1016/j.soildyn.2011.07.001

the Damage Mechanics Model in the framework of Continuum Mechanics [7–9] are the most typical. In addition to those models mentioned, XFEM and crack-embedded element [10] can simulate strong discontinuity in material, DEM [11], DDA [12], rigid body-spring element [13] model structure with pre-defined blocks and can study the relative motion between blocks.

Seismic failure process analysis of high concrete dams is a very complicated problem. In strong earthquake shocks, the dam may go through the whole process of elastic deformation, initiation and propagation of cracks, severe damage and ultimate failure. The numerical model should adequately reproduce this strong nonlinear process and has the potential to incorporate various factors including complex geometry of the dam, partitioning of concrete, flexibility of foundation, dam–reservoir interaction, opening/closing of contraction joints and so on. In addition, time marching process of thousands of time steps also poses a harsh challenge to computational capacity. Existing research fell short in certain aspects. Furthermore, it is worthwhile to point out that concrete has always been assumed as homogeneous in seismic analysis of concrete dams, which is not representative of the reality.

Prof. C.A. Tang considers that the nonlinearity of concrete is caused by microcracks instead of plasticity. He developed the failure process model for rock (RFPA) [14,15], and introduced this model to analyse the concrete specimens thereafter. The concrete is simulated by three phases—coarse and fine aggregates, mortar and the interfaces between them; heterogeneity of each phase is considered by a random distribution of material properties. Complicated failure process and failure modes of concrete specimens in the shape of cubes and beams have been obtained and resemble those of lab tests. Tang's work mainly focuses on static response of laboratory specimens, while cases of practical engineering structures subjected to cyclic loading are not available in the literature till now.

In the present paper, Tang's model has been extended to seismic failure modeling of high concrete dams. The obtained failure mode of an arch dam is in accordance with that of the shaking table test. Based on that, the failure process and the failure modes of a gravity dam are investigated. New perspectives are provided regarding the seismic failure of gravity dams.

2. Model for failure analysis of concrete dam

2.1. Consideration of heterogeneity of concrete

Dam concrete is heterogeneous in nature, with substructures such as coarse and fine aggregates, mortar and so on. In conventional analysis of dams, concrete has always been assumed to be homogeneous. For methods in the framework of FEM, the dam is discretized with elements with sizes ranging from several meters to tens of meters. Nonlinear constitutive relations are assumed for these elements. Complicated theory and programming are required, and distribution of displacement/stress response of the dam is generally obtained.

Tang's RFPA focuses on simulation of failure process of rock/concrete specimens in laboratories. Concrete is divided into three phases—coarse and fine aggregates, mortar and the interfaces between them on the mesoscopic level. Each phase is considered to be an elasto-brittle material. Failure of concrete is regarded to be caused by micro-cracking in it, which is described by stiffness degradation. Tang's success in reproducing some physical concrete test results provides us the possibility to arrive at failure mechanism of material or structure from a lower scale.

However, as far as high dams are concerned, it is far from realistic to model exactly all substructures of concrete in seismic analysis. Yet it is also unnecessary. So some simplifications are introduced. Most important of all, the dam is discretized with finite elements, and the three phases, i.e. matrices, aggregate and interfaces, may coexist in each single element. For each element, all substructures in it are blended, resulting in an equivalent homogeneous element, with its material properties decided by the original substructures. If element sizes are small enough, this process would result in different properties for elements containing different contents of substructures. In the next step, the finite element model of dam is viewed as a sample space. If there are plenty of samples in this space, in other words, the dam is discretized with plenty of finite elements, the material properties of elements can be assumed to conform to some specific distribution, such as the Weibull distribution. In this way, the heterogeneity of concrete can be reflected to some degree. The size of elements employed should be small enough so that the substructures contained in each element cause difference in the material properties when compared to the average value.

As stated above, material properties of all elements in the model are assumed to conform to a certain random distribution. Here the Weibull distribution law based on the weak link theorem is employed, whose probability density function is as follows:

$$f(x) = \frac{m}{x_0}\left(\frac{x}{x_0}\right)^{m-1} e^{(-x/x_0)^m} \tag{1}$$

Here x is the variant that conforms to the Weibull distribution (Fig. 1) and x_0 converges to the average value when the sample space is highly homogeneous. m quantifies the degree of heterogeneity of all samples in the sample space. To be specific, assume that x stands for the elastic modulus of an element in the finite element model of the dam, then x_0 is similar to the average elastic modulus. A smaller m indicates a heterogeneous dam while a bigger m implies a more homogeneous dam concerning elastic modulus.

Corresponding to the probability density function curves shown in Fig. 1, Fig. 2 presents the distribution of elastic modulus of the dam for a different m. Colors ranging from white to black are used to depict the value of elastic modulus of elements. Lighter color stands for higher modulus while darker color stands for lower modulus. Obviously the smaller the m, the more heterogeneous the dam concerning modulus, and vice versa. For other material properties such as compressive strength, Poisson's ratio, mass density, etc., similar figures can be obtained.

It is necessary to mention that since there is no existing research for quantification of concrete homogeneity by random distribution through theoretical deduction or experiments, determination of m in this manuscript lacks solid theoretical or experimental background. This is acceptable for an exploratory research. With the on-going research, it can be expected that determination of m will be more rational.

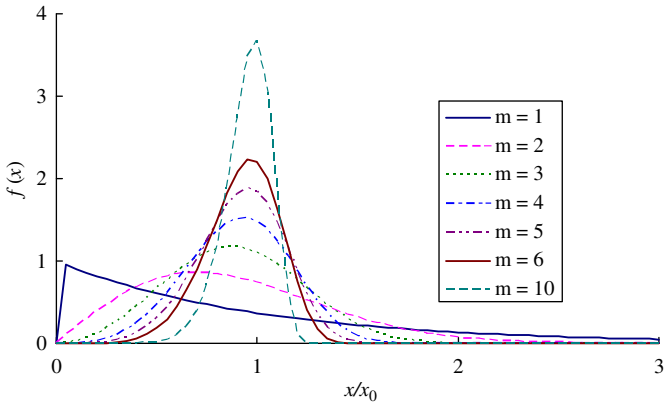

Fig. 1. Probability density function of the Weibull distribution.

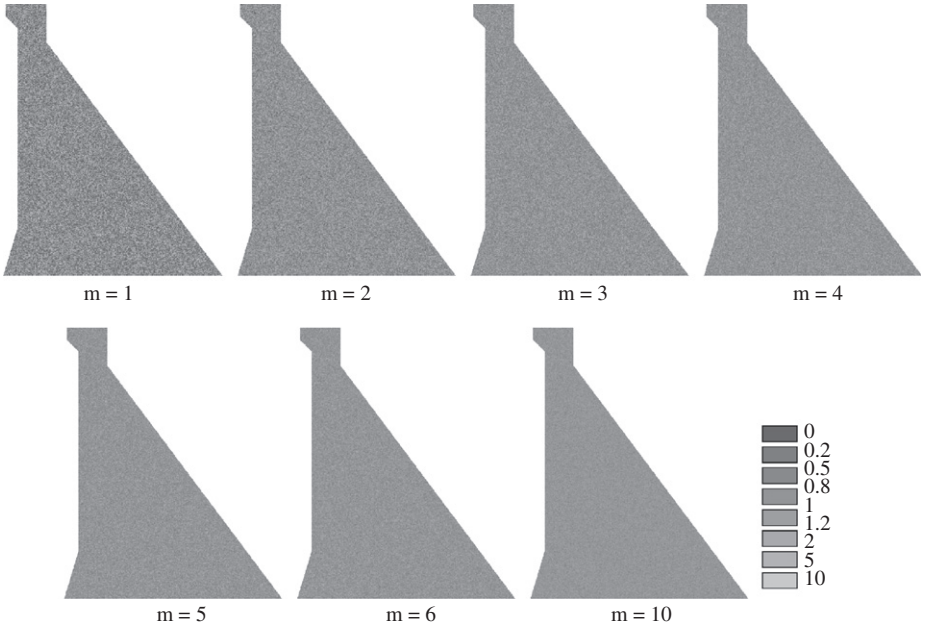

Fig. 2. Distribution of elastic modulus in the FE model of the dam.

2.2. Constitutive relation and failure criterion

As stated in many literatures, the nonlinearity of concrete is closely related to initiation and propagation of microcracks, instead of plasticity. Concrete exhibits the feature of elaso-brittle materials on the mesoscopic scale. Substructures in the concrete fail and lose bearing capacity when strength of the substructure is exceeded. These substructures fail one by one, so initiation and propagation of microcracks take place.

Since the size of elements is small although not strictly on the mesoscopic level, elastic damage constitutive relations (Fig. 3) are assumed for the elements. When the tensile strength of the element is reached, tensile damage occurs and the stress–strain curve descends linearly until the residual strength is reached, when the element is assumed to have suffered serious damage and its strength falls to the constant residual value. Ultimate strain is the limit for the stress–strain curve, and a totally damaged element is resulted when its tensile strain is greater than ultimate strain. Considering the fact that element size is not really on the mesoscopic level, as compared to Tang's elasto-brittle constitutive relation, descending section is introduced to the stress–strain relation.

The evolution law of tensile damage is as follows. The tensile damage D_t is decided according to ε_t, the principal tensile strain of the element:

$$D_t = \begin{cases} 0 & \varepsilon_t < \varepsilon_{t0} \\ 1-\left(\frac{\lambda-1}{\eta-1}+\frac{\eta-\lambda}{\eta-1}\frac{\varepsilon_{t0}}{\varepsilon_t}\right) & \varepsilon_{t0} \le \varepsilon_t < \varepsilon_{tr} \\ 1-\frac{\lambda\varepsilon_{t0}}{\varepsilon_t} & \varepsilon_{tr} \le \varepsilon_t < \varepsilon_{tu} \\ 1 & \varepsilon_t \ge \varepsilon_{tu} \end{cases} \quad (2)$$

Here ε_{t0}, ε_{tr} and ε_{tu} imply the elastic strain limit, threshold for the residual section and the ultimate strain, respectively. η and λ are the two parameters. η characterizes the range of the descending section with $\eta=\varepsilon_{tr}/\varepsilon_{t0}$; smaller η implies a steeper curve. Since ε_{t0} is greater than or equal to ε_{tr}, $\eta \ge 1$ is assumed. Parameter λ stands for the ratio between residual strength f_{tr} and f_t; larger λ implies the stronger bearing capacity of the element after being damaged.

The constitutive relation of element in compression is shown in Fig. 4. As can be seen, the linear section is followed by a power function shaped curve. ε stands for compressive strain in uniaxial compressive loading, while in multiaxial loading case, ε is replaced by an equivalent strain $\bar{\varepsilon}=-\sqrt{\langle-\varepsilon_1\rangle^2+\langle-\varepsilon_2\rangle^2+\langle-\varepsilon_3\rangle^2}$. ε_{c0} and ε_{cu} are the elastic strain limit and the ultimate strain, respectively. f_c is the compressive strength of the concrete element.

As similar to Tang's model, the Mohr–Coulomb criterion with tension cut-off is employed as the failure criterion. So both tensile

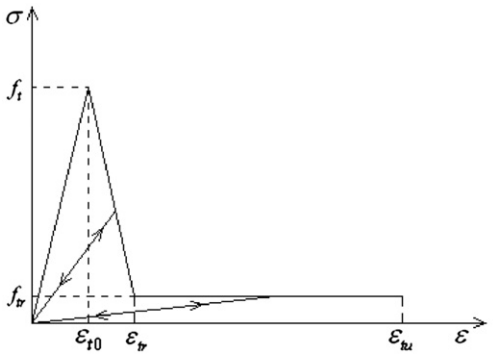

Fig. 3. Stress–strain curve for concrete in tension.

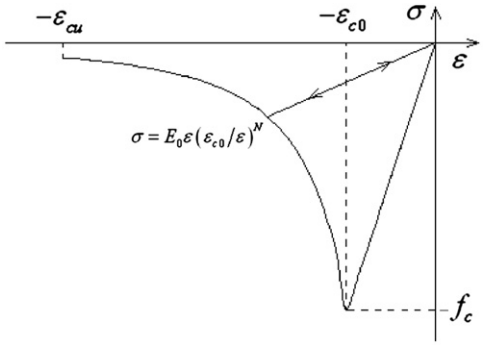

Fig. 4. Stress–strain curve for concrete in compression.

damage and shear damage are possible for elements. Considering the fact that the tensile strength of concrete is much lower than compressive strength and seismic damage of concrete dams is caused mainly by cracking instead of crushing of concrete, the determination of tensile damage has priority over that of shear damage. In a single iteration, once tensile damage occurs in the element, no shear damage will be assumed any more. Both tensile damage and shear damage are irrecoverable, but tensile damage does not affect the compression bearing capacity of the element. In other words, a totally cracked element can still sustain the compressive loading. While on the contrary, compressive damage affects the tension bearing capacity of the element, and crushed element can sustain neither compression nor tension any more.

2.3. Relation between material parameters on the mesoscopic scale and macroscopic scale

Owing to the consideration of heterogeneity, weak links are introduced into the concrete. This is easy to understand simply by comparing the loading capacity of two concrete cube samples discretized with finite elements. The first one is homogeneous with a tensile strength of f_0, so the bearing capacity of the cube subjected to uniaxial loading is $f_0 * A$, with A indicating the area of section of the cube. The other is heterogeneous with modulus and strength of elements conforming to the Weibull distribution with a heterogeneity index m, so in this way some elements in the cube have tensile strengths lower than f_0, which become weak links when subjected to loading. As a result, the bearing capacity of the latter is lower than $f_0 * A$. So revision has to be made toward material properties of elements in the heterogeneous cube to make sure both cubes have the same bearing capacity and modulus when subjected to uniaxial loading.

Take a cube with the dimension of 10 cm × 10 cm × 10 cm as an example. The cube is discretized with elements having the length of 1 mm, which is a proper size to reflect the mesoscopic structures contained in the cube. The modulus and compressive strength of these elements conform to the Weibull distribution with a heterogeneity index m. Since Poisson's ratio and density are not influenced much by the heterogeneity on the mesoscopic level, they are assumed to be constants. The bearing capacity of the cube subjected to uniaxial tensile loading can be obtained by performing nonlinear analysis with the proposed procedure, and then the average tensile stress of the cube can be achieved. This stress corresponds to the uniaxial tensile strength of the cube, and it is named as the macroscopic tensile strength here. Similarly, macroscopic elastic modulus can be obtained from the initial slope of the average stress–average strain curve of the cube.

Strength coefficient C_F and elastic modulus coefficient C_M are defined by dividing the x_0 (namely mesoscopic material properties here, including strength and modulus) by its corresponding macroscopic strength and macroscopic modulus. Owing to introduction of heterogeneity of material properties into the cube, weak links are introduced as well, so the macroscopic values are smaller than its counterpart on the mesoscopic scale. But with an increasing m, both coefficients converge to unity.

Cases of $m=1, 2, 3, 4, 5, 6$ and 10 are considered, with strength coefficient and modulus coefficient plotted in Fig. 5. In order to be consistent with the numerical examples in Section 3, three indices of concrete (C15, C20 and C25) are considered, and for each concrete index, three cube samples for each m are generated and computed to minimize the influence of a random distribution of parameters. As can be seen from the figure, for a larger m, the macroscopic properties are more close to the corresponding mesoscopic values. Concrete index hardly influences the strength coefficient. Concerning the modulus, when m is smaller than 2, the concrete index causes obvious difference in C_M, but for $m \geq 2$, it

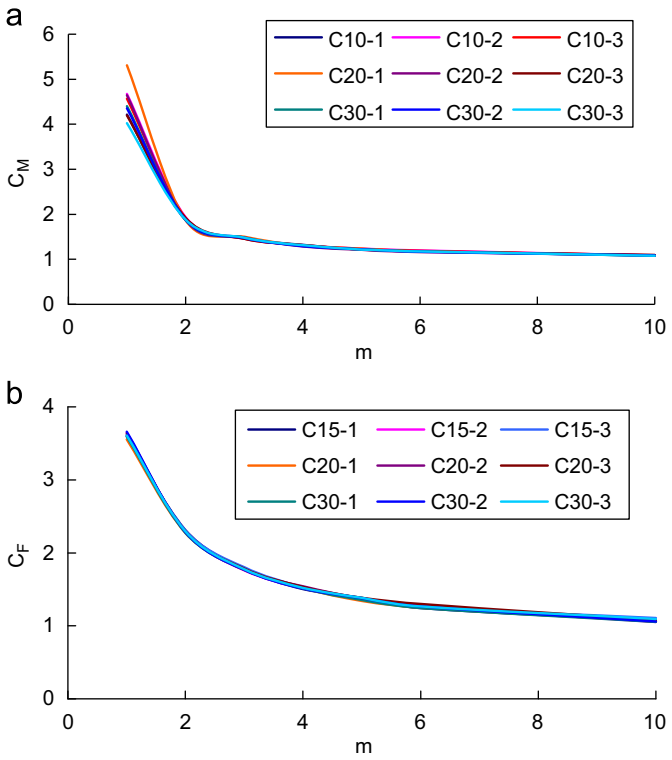

Fig. 5. Relation between material properties on the macroscopic scale and on the mesoscopic scale. (a) Modulus and (b) tensile strength.

exerts little influence on C_M. This phenomenon greatly facilitates practical application to dams constructed with concrete of different indices since for m not smaller than 2, uniform relations of C_F–m and C_M–m are available.

In the damage simulation in Sections 3 and 4, the tensile strength and modulus of elements after considering heterogeneity of concrete are revised according to m with the strength coefficient C_F and the elastic modulus coefficient C_M presented here. This guarantees that elements considering heterogeneity are equivalent to their counterparts of homogeneous elements concerning uniaxial tensile strength and modulus, for m ranging from 1 to 10.

2.4. Simulation of seismic damage of concrete dams

Prior to seismic loading, the dam has already been subjected to static loadings including self-weight, hydrostatic pressure, uplift pressure, sediment pressure, temperature change, etc. Dam subjected to static loading is assumed as the initial state, and the damage due to static loadings is considered. The static stress field as well as strain field and displacement field are assumed to be constant considering the fact that seismic excitation is of short duration.

Seismic loading is excited on the dam in the initial state. In each time step of the seismic excitation, the equation of motion of the dam–foundation system is solved to obtain the displacement field and stress–strain fields, based on which damage calculation of elements in the dam is performed. Then the double convergence criterion is employed for convergence check. To be specific, if no new damage of elements is present, the analysis of the present time step is finished. Here new damage refers to damage caused to originally undamaged elements or more serious damage caused to damaged elements. Otherwise, if either number of newly damaged elements or displacement variation relative to the previous iteration exceeds the pre-defined threshold (number of newly damaged elements: 5; 2 norm of displacement: 1%),

stiffness of damaged elements is updated and another iteration is performed. Iteration in the same time step is required until the double convergence criterion is met, when calculation of the next time step can be started.

Since the dynamic failure process analysis costs great computational effort, fast and efficient time marching process should be employed. In addition, the degradation of element stiffness together with the opening/closing of cracks brings about strong nonlinearity to the analysis, so algorithm damping is required to dissipate fictitious high vibration modes in order to guarantee the convergence and stability of the algorithm.

For this purpose, the single step α-Newmark procedure proposed in the literature [16] and improved SSOR-PCG [17] solver are employed.

The presented model has the advantage that the discontinuous nature of cracks can be modeled in a continuous way. For totally damaged elements due to tension, i.e. the damage index D reaches 1, implying a totally damaged element, the modulus of the element is assumed with a sufficiently small value in tension state. As compared to the undamaged elements, the influence of totally damaged elements in the overall stiffness matrix is negligible. From a physical point of view, these elements become very soft and can deform in a wide range, exerting negligible influence on the elements adjacent to them. While for totally damaged elements due to tension, they can still sustain compressive loading. So when compressive stress is detected in these elements, their modulus is recovered, thus recovering the capacity for compressive loading. This is also representative of the reality. So the treatment of the totally damaged elements is reasonable to approximate the effect of cracks; yet no knowledge is required concerning the cracking route beforehand and remeshing due to crack propagation and other complicated formulae to model discontinuity are not necessary. Propagation, coalescence and bridging of cracks can be modeled conveniently.

Computational code has been programmed based on the aforementioned procedure by the authors [18]. The code has two versions: serial computing code and parallel computing code. With either version the whole process of the dam from elasticity to minor damage, and then to crack initiation and propagation, which finally leads to dam failure can be obtained. The parallel code can handle more degrees of freedom when running on a parallel platform.

3. Validation of the model

A practical arch dam is used to validate the proposed model. The dam is a double-curvature one, with a height of 210 m and a design PGA of 0.5575 g. The shaking table test has been performed on models of this dam in the Dalian University of Technology and failure modes have been recorded. More details of the test can be referred to in Ref. [18].

Shown in Fig. 6 is the setup of the experiment. The dam and a small portion of foundation adjacent to the dam have been modeled. The geometry scale is 1/273. A type of similitude concrete with low elastic modulus and low strength is used to cast the model. The acceleration scale is 1.0 since the test is performed in constant gravity field. Acceleration time history with an amplitude of 1.0 g is generated from the spectrum (Fig. 7) as specified in the Specifications for Seismic Design of Hydraulic Structures [1], and is input in the upstream direction of the dam. To simplify the setup of the experiment, an empty reservoir is assumed.

With the on-going shaking, cracks initiate and propagate at the dam crest near the cantilever, causing three concrete blocks to fall off the dam body one by one. The final failure mode of the dam is shown in Fig. 8. A breach with a height of one-fifth of the dam and a width of one-third of the dam crest is observed on top of the dam, while the rest of the dam and the foundation remain stable and no cracks are observed.

Fig. 6. Setup of the experiment.

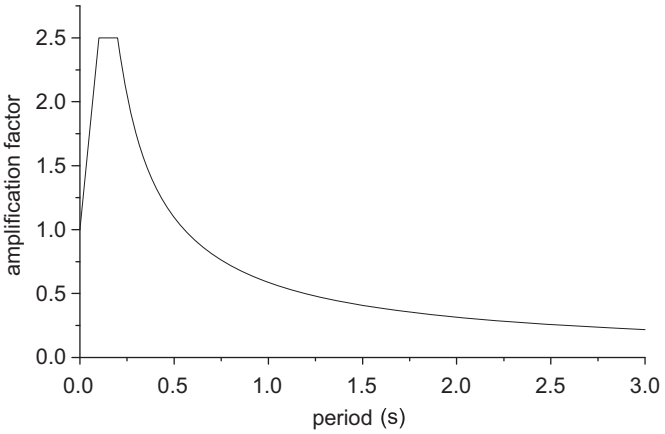

Fig. 7. Acceleration spectrum.

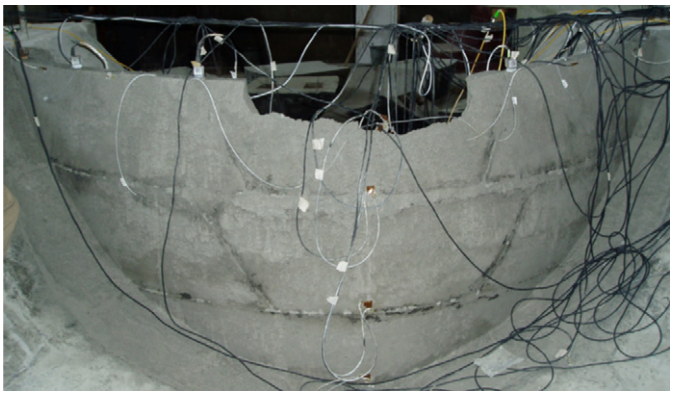

Fig. 8. Failure mode of the dam.

The failure mode of the arch dam with similar situation in the test is modeled by numerical analysis. The finite element discretization of the dam–foundation system is shown in Fig. 9. Since 358,956 elements and 386,276 nodes are used to discretize the system resulting in more than one million degrees of freedom, parallel computing has to be employed for the computation. Different colors of elements denote domain decomposition in parallel computing and elements of different colors are allocated to different processors in the parallel platform.

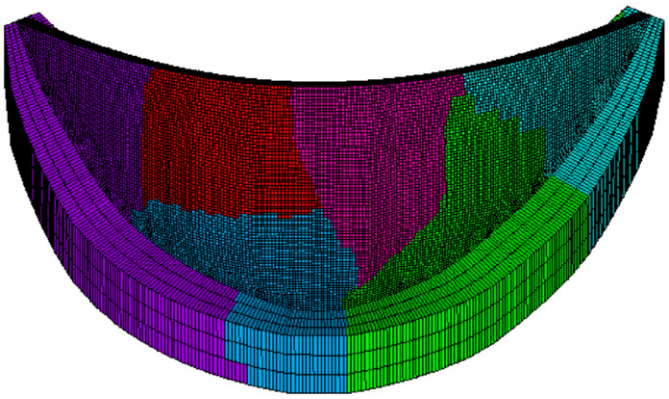

Fig. 9. Finite element discretization of the arch dam–foundation system.

Table 1
Material property of concrete.

Modulus (GPa)	Poisson's ratio	Density (kg/m^3)	Compressive strength (MPa)	Tensile strength (MPa)
24.0	0.17	2400	30.0	3.0

Table 2
Parameters in the constitutive relation for the dam.

Type of constitutive relation	Parameters			
Tension	η 1.0	γ 0.2	ξ 10	λ 0.05
Compression	N 4	ξ 100	λ 0.2	

The same parameters for material properties are assumed for the dam and the foundation (Table 1), only that the foundation behaves linearly in order to save computational effort since no cracks are observed in the test. The required parameters in the constitutive relation for the dam part are listed in Table 2.

An empty reservoir is assumed, so only self-weight of concrete and acceleration excitation are considered for the loading situation. Acceleration time history with an amplitude of 1.0 g is input in the upstream direction.

Since acceleration time history is introduced in the stream direction, the tensile stress in the region near the cantilever top is the highest. Two vertical cracks at the edge of block 1 in Fig. 10 initiate and propagate downward, causing release of tensile stress in the arch direction and increase in tensile stress in the cantilever direction. With the on-going vibration, the lower crack forming block 1 is observed and block 1 is finally detached from the dam body. Then a horizontal crack occurs at the left side of block 1 and propagates leftward. Stress redistribution causes the emergence of a vertical crack at the end of the horizontal crack. Both cracks bridge and block 2 gets separated from the dam body. The cause for block 3 is similar to block 2. The final failure mode of the dam is shown in Fig. 10, which resembles the test result shown in Fig. 8 quite a lot. Fig. 11 shows location of damaged elements and their relative energy release, indicated by sizes of balls.

4. Numerical examples

A concrete gravity dam named Jin'anqiao Dam being built in China on the Jinshajing River is employed to model its seismic damage process. It is a Roller Compacted Concrete Dam and the maximum height is 160 m. The non-flow section considered is about 114 m. The design PGA is 0.399 g.

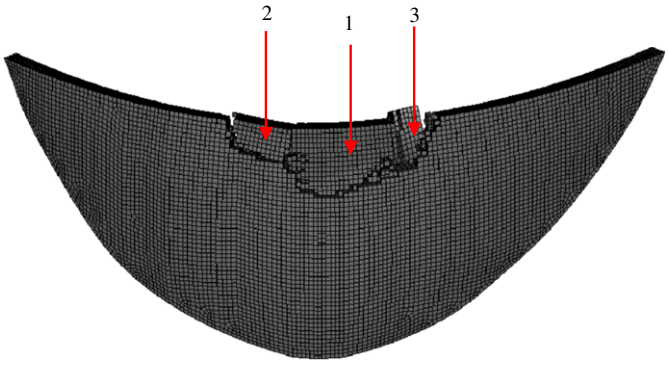

Fig. 10. Failure mode of the arch dam.

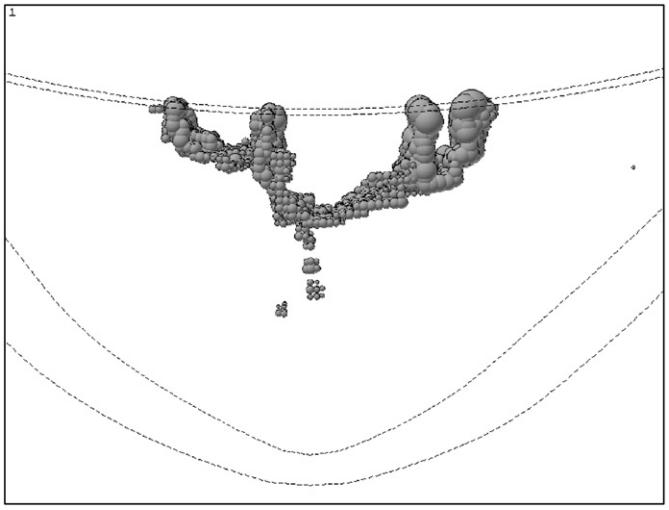

Fig. 11. Failed elements in the dam (upstream view).

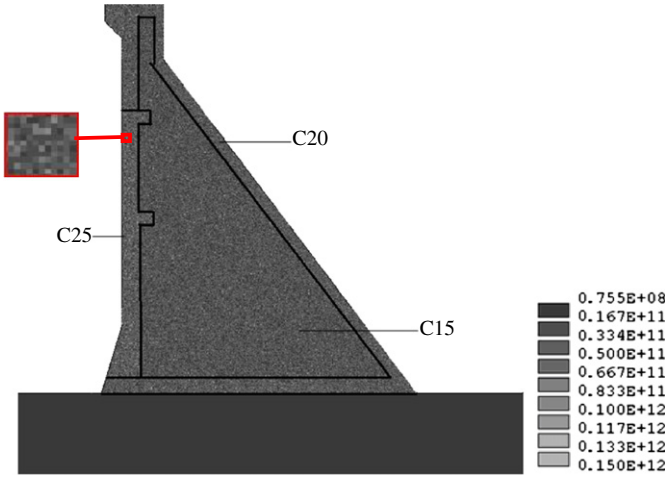

Fig. 12. FE discretization and modulus distribution of the dam.

4.1. FEM model and material properties

The dam is discretized with quadratic plane strain elements, with the maximum element size of 0.3 m. This results in 59,665 elements and 60,260 nodes in all for the dam (Fig. 12).

Foundation corresponding to twice the dam height from the dam heel to upstream, from the dam toe to downstream and from the dam bottom downward is modeled with massless foundation. The outer boundary of the foundation is constrained. Since the presented research aims at damage process of the dam, heterogeneity and nonlinearity of the foundation rock are not considered. Fine elements near the dam transit gradually to coarse elements far away from the dam, with the maximum size less than 10 m.

Conventional concrete and RCC concrete are both employed to cast the dam. Three indices of concrete are employed, i.e. C15, C20 and C25. The static material properties are listed in Table 3. The heterogeneity indices m of modulus and compressive strength are assumed to be 2, since no experiment results are yet available on how heterogeneous concrete is. The tensile strength is taken as 10% of its compressive counterpart. The material properties of the foundation rock are listed in Table 4. To account for the effect of strain rate, modulus and strength for the dam and modulus for the foundation rock are increased by 30% according to the Code for Seismic Design of Hydraulic Structures in China. Parameters in the constitutive relations shown in Figs. 3 and 4 are listed in Table 5.

In order to minimize the influence of randomness in generating random numbers for the modulus and strength, thirty samples of the dam considering heterogeneity are generated. All of the samples are generated from the same parameters shown in Table 3, but with different seeds in generation of random numbers ranging from zero to one, based on which random numbers conforming to the Weibull distribution are generated. One of the samples as well as the meshes is shown in Fig. 12. The gray color in the figure implies the value of modulus, with lighter color standing for higher modulus. Elements with modulus much higher or much lower than the average value are all possible in the model. Partitioning of different indices of concrete is also shown in the figure. As can be seen, the color for concrete elements of index C25 is generally lighter than that of C15 and C20.

Rayleigh damping has been used and the damping ratios for all modes of vibration are 5%. A full reservoir with water level 10 m lower than the dam top is assumed. Effect of hydrodynamic pressure is approximated by Westergaard's added mass model.

For comparison, in addition to the model considering both heterogeneity and nonlinearity of concrete, which will be referred to as Model I later, two more sets of models are considered. In Model II, both heterogeneity and nonlinearity of the dam concrete are neglected. In Model III, the same thirty dam samples as in Model I are adopted, so heterogeneity of concrete is considered but concrete is assumed to be a linear elastic material.

4.2. Earthquake excitation

Artificial acceleration time histories are generated from the site-specific spectrum of the project. Both stream direction and vertical direction are subjected to earthquake excitation and the normalized acceleration time histories are plotted in Fig. 13. Owing to the uncertainty of earthquake activities, the amplitude of earthquakes may vary over a wide range according to the seismic hazard analysis with a different occurrence probability. Six levels of acceleration amplitudes are employed in the analysis, i.e. 0.2g, 0.3g, 0.399g, 0.5g, 0.6g and 0.8g. So the normalized acceleration time histories are multiplied by the six amplitudes to generate six groups of acceleration excitations.

4.3. Vibration mode

Modal analysis is performed on the dam samples of Models I and II. For Model III, since the same dam samples as in Model I are adopted, their vibration modes are the same as Model I. For Model I, all the thirty samples are considered. So thirty-one models are analyzed in all and the first five natural frequencies and vibration modes for each model are obtained. Resemblance is observed for their vibration modes and result of only one model is presented in Fig. 14. The first five natural frequencies of the 31 models (thirty for Model I and one for Model II) are listed in Table 6.

As far as natural frequency is concerned, quite similar results are obtained for all the thirty samples for Model 1. The coefficients of variation for the five sets of frequencies are $7.67e^{-5}$, $1.07e^{-4}$, $2.79e^{-4}$, $1.13e^{-3}$ and $1.36e^{-3}$. This indicates that although the material properties of these dam samples differ from each other owing to random distribution, similar dynamic properties of dams are maintained. When compared with Model II, in which the dam is assumed to be homogeneous, dam samples in Model I turn out to be slightly flexible. The natural frequencies are similar, with an average difference for the five sets of frequencies of 2.24%, 2.04%, 2.60%, 3.34% and 3.81%. So it can be justified that the dynamic properties of the dams considering heterogeneity of concrete are comparable with that of the dam assuming homogeneous material properties. This is a solid foundation for reasonable comparison of nonlinear seismic response between them.

Table 4
Material property of the foundation rock.

Modulus (GPa)	Poisson's ratio	Density (kg/m^3)
16.5	0.25	2550

Table 5
Parameters in the constitutive relation.

Type of constitutive relation	Parameters			
Tension	η	γ	ξ	λ
	1.0	0.2	10	0.05
Compression	N	ξ	λ	
	4	100	0.2	

Table 3
Material properties of the dam.

Concrete	Macroscale parameters			Heterogeneity index			Parameters considering heterogeneity		
	C15	C20	C25	C15	C20	C25	C15	C20	C25
Modulus (GPa)	22	25.5	28	2	2	2	41.98	48.03	52.54
Poisson's ratio	0.17	0.17	0.17	/	/	/	0.17	0.17	0.17
Density (kg/m^3)	2400	2400	2400	/	/	/	2400	2400	2400
Compressive strength (MPa)	15	20	25	2	2	2	34.29	45.79	57.43
Tensile strength (MPa)	1.5	2.0	2.5	2	2	2	3.429	4.579	5.743

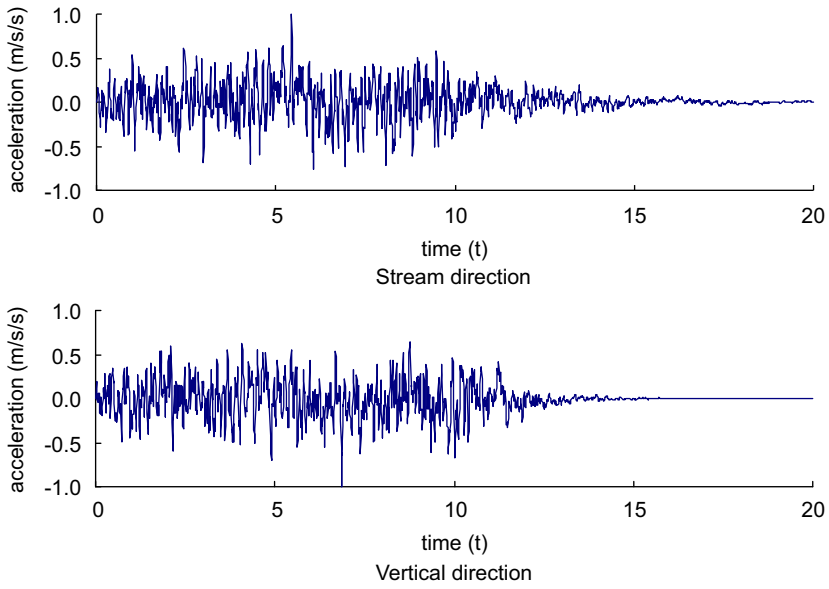

Fig. 13. Earthquake excitation (normalized).

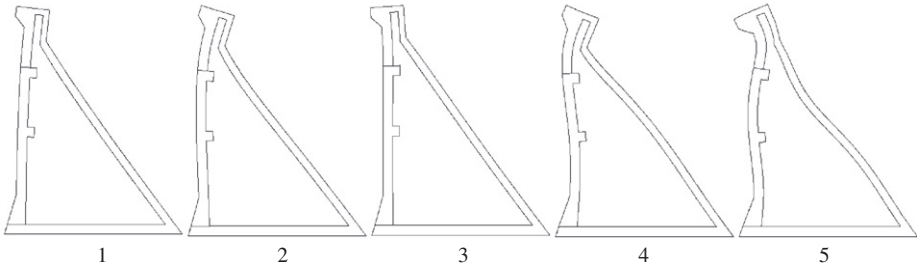

Fig. 14. First five vibration modes of the dam.

Table 6
Natural frequencies for the dam–foundation system.

	Model	Set of frequency						Model	Set of frequency				
		1	2	3	4	5			1	2	3	4	5
Model I	1	2.09	4.48	5.21	8.18	11.61	Model I	16	2.09	4.48	5.21	8.18	11.61
	2	2.09	4.48	5.22	8.19	11.60		17	2.09	4.47	5.20	8.15	11.60
	3	2.10	4.48	5.21	8.17	11.59		18	2.09	4.48	5.21	8.18	11.60
	4	2.09	4.48	5.22	8.21	11.64		19	2.09	4.47	5.22	8.20	11.61
	5	2.09	4.48	5.21	8.20	11.60		20	2.09	4.48	5.21	8.19	11.66
	6	2.09	4.47	5.21	8.19	11.61		21	2.09	4.47	5.21	8.16	11.57
	7	2.09	4.47	5.19	8.15	11.59		22	2.09	4.48	5.21	8.20	11.61
	8	2.09	4.48	5.21	8.18	11.59		23	2.09	4.48	5.21	8.19	11.59
	9	2.09	4.48	5.21	8.19	11.59		24	2.09	4.47	5.21	8.22	11.65
	10	2.09	4.47	5.20	8.16	11.60		25	2.09	4.48	5.21	8.18	11.61
	11	2.10	4.48	5.22	8.21	11.65		26	2.09	4.47	5.22	8.22	11.61
	12	2.09	4.48	5.21	8.18	11.62		27	2.10	4.49	5.22	8.20	11.66
	13	2.09	4.48	5.22	8.20	11.61		28	2.09	4.48	5.22	8.21	11.65
	14	2.09	4.48	5.21	8.18	11.60		29	2.09	4.48	5.21	8.19	11.61
	15	2.09	4.47	5.20	8.16	11.59		30	2.09	4.47	5.20	8.19	11.58
Model II		2.14	4.57	5.35	8.47	12.07							

4.4. Seismic damage process and failure modes

Since thirty dam samples considering heterogeneity and acceleration time histories corresponding to six amplitudes are considered, 180 groups of response of the dam are obtained. A typical damage process of the dam subjected to acceleration time histories with an amplitude of 0.6 g, about 1.5 times the design PGA, is plotted in Fig. 15.

When the dam is loaded with only static loads, stress level in the dam is relatively low, only several elements are damaged and no visible crack is detected. With the on-going acceleration excitation, the dam heel as well as upstream surface and downstream surface

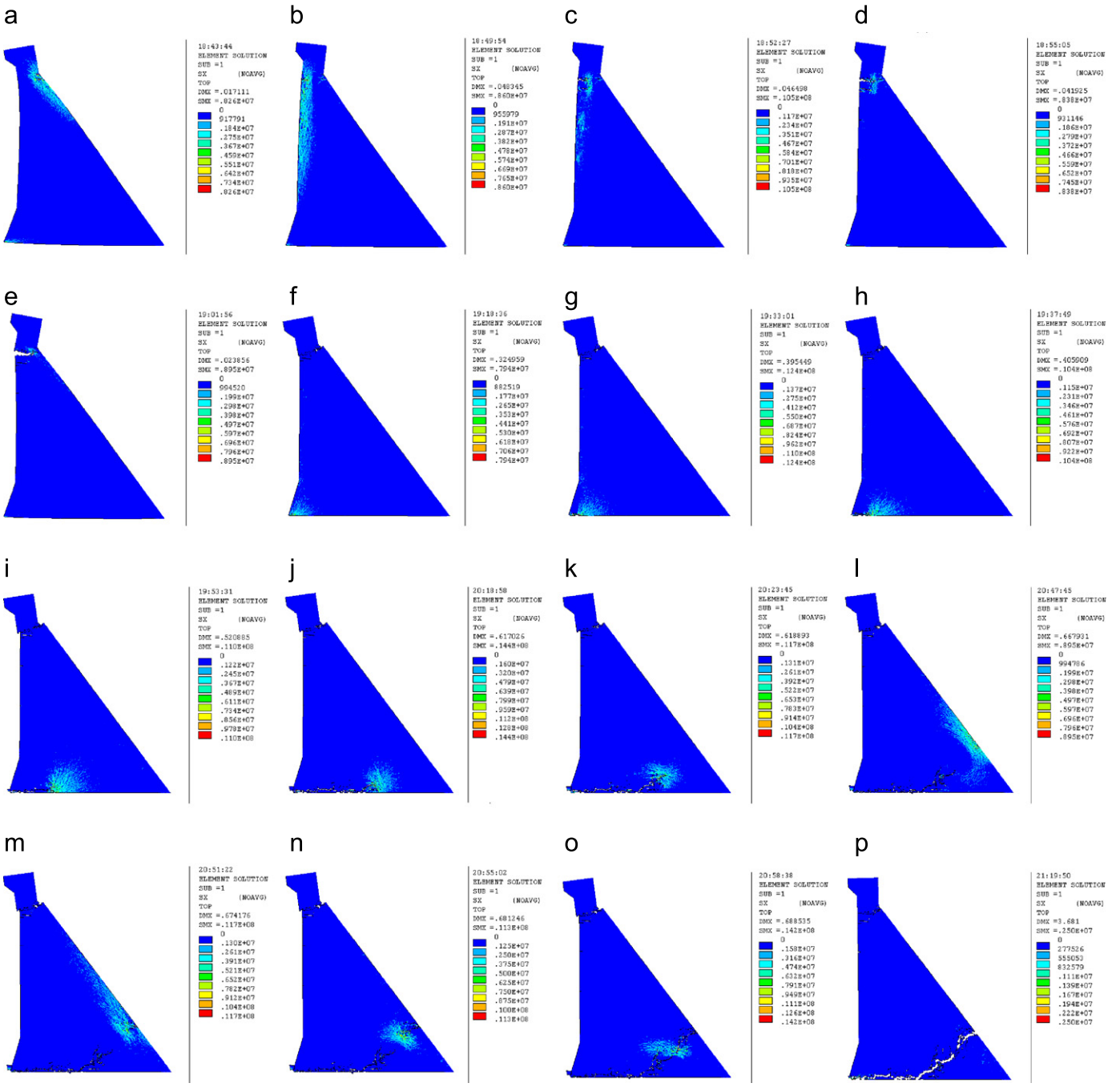

Fig. 15. A typical damage process of the dam. (a) 2.05 s, (b) 2.1 s, (c) 2.14 s, (d) 2.17 s, (e) 2.47 s, (f) 2.73 s, (g) 3.52 s, (h) 3.68 s, (i) 4.01 s, (j) 4.52 s, (k) 4.63 s, (l) 4.99 s, (m) 5.24 s, (n) 5.35 s, (o) 5.50 s and (p) 6.31 s.

of the dam are characterized by high tensile stress and compressive stress, but still no visible crack occurs. At 2.05 s, however, the dam vibrates in the upstream direction and two short cracks appear near the dam neck in the downstream surface, and the maximum tensile stress at the crack tip is 8.26 MPa (Fig. 15(a)). Then when the dam vibrates rigorously in the downstream direction, several short cracks appear in the upstream surface, with two near the dam neck (Fig. 15(b)–(d)). During the next seconds, these two cracks propagate horizontally quickly and finally meet the aforementioned short cracks at the downstream surface at 2.47 s, causing the dam head detached from the dam body (Fig. 15(e) and (f)). The other short cracks on the upstream face remain stable until the computation ends.

At 3.52 s, horizontal crack appears at the dam heel and tensile stress is remarkably concentrated here, with a maximum tensile stress of 12.4 MPa (Fig. 15(g)). With the continuous vibration of the dam, this crack continues to grow toward downstream. However, the crack is not strictly along the dam bottom. Instead, it kinks into the dam and then gets back to the bottom now and then, accompanied by small cracks near the main crack (Fig. 15(h)–(j)). At 4.63 s, the crack gets into the dam concrete at an angle of about 40° with respect to the dam bottom (Fig. 15(k)). The stress state of the dam is greatly influenced since the section of the cantilever is remarkably changed due to the crack. A new high-stress zone is developed on the downstream surface at 4.99 s, with its approximate location decided by extending the inclined crack to intersect

with the downstream face (Fig. 15(l)). So a new crack initiates and propagates almost perpendicular to the downstream surface at 5.24 s (Fig. 15(m)). The tips of this crack and the aforementioned inclined crack are characterized by high tensile stress and they finally bridge at 5.50 s (Fig. 15(n) and (o)). Till now, only a small portion of concrete near the dam toe remains stable and the dam body is totally detached from it. Up till the end of the time history, a residual displacement of about one meter for the detached body from the remaining body exists. No additional major crack has grown and the configuration of the dam remains as it has been at 6.31 s (Fig. 15(p)).

From the 180 numerical simulations, four typical failure modes are obtained, as shown in Fig. 16. The first failure mode (Fig. 16(a)) is cracking at the dam neck. The second mode (Fig. 16(b)) is cracking that initiates from the dam heel and propagates horizontally a certain distance toward downstream. Several short cracks may occur on the dam faces but do not propagate through the dam. Only a few of them evolve into dominant cracks. These two failure modes can be caused by relatively minor earthquakes. Since water pounding function of the reservoir is retained to a great extent, no disastrous results would occur toward the downstream areas. In the third failure mode (Fig. 16(c)), cracks initiate from the dam face, which is especially easy for dam face where slope changes abruptly, and propagate deep into the dam and finally reach the dam face at the other side. In the fourth failure model (Fig. 16(d)), the crack at the dam bottom propagates toward downstream and reaches the downstream face. The crack does not follow the dam–foundation interface all the way but inclines approximately perpendicular to the downstream face after propagating horizontally for a certain distance. This is due to the reason that the stress state changes from tension-shear to compression-shear in the propagation process of crack. These two failure modes require much stronger vibration (maybe twice the design PGA or even greater than that) as compared to the former two modes. Although earthquake shocks much stronger than the design value are of low probability, the experiences from the Shapai Arch Dam in the Wenchuan earthquake showed that this could happen. Dams failed in these two modes will cause serious disaster to the downstream areas owing to the loss of water pounding function, and definitely merit more attention from the dam designers and related researchers.

The nonlinear analysis is performed on a personal computer, with a configuration of 3 GB CPU with four cores, 2 GB RAM and 500 GB hard disk. The elapsed time varies with a degree of nonlinearity of the dam, and more elements getting damaged obviously require more nonlinear iterations for convergence. On average, twenty hours are necessary for computation of one dam sample subjected to one complete time history of 20 s with a time step of 0.01 s, of which the performance is quite satisfactory and meets the requirement for engineering practice.

4.5. *Influence of heterogeneity and nonlinearity of concrete*

The influence of heterogeneity of concrete as well as nonlinearity of concrete is investigated by performing the same analysis to Models I–III. Similar material properties and loading case are assumed for Models II and III as that for Model I, whose result is shown in Fig. 15. The maximum tensile stress obtained in the time history is shown in Fig. 17.

The influence of heterogeneity of concrete can be addressed by comparing Fig. 17(b) and (c). The overall distribution of tensile

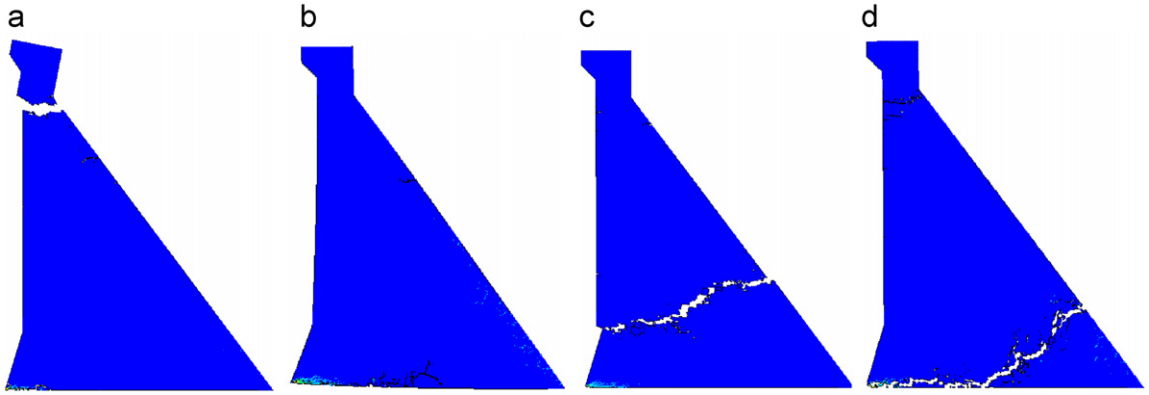

Fig. 16. Typical failure modes.

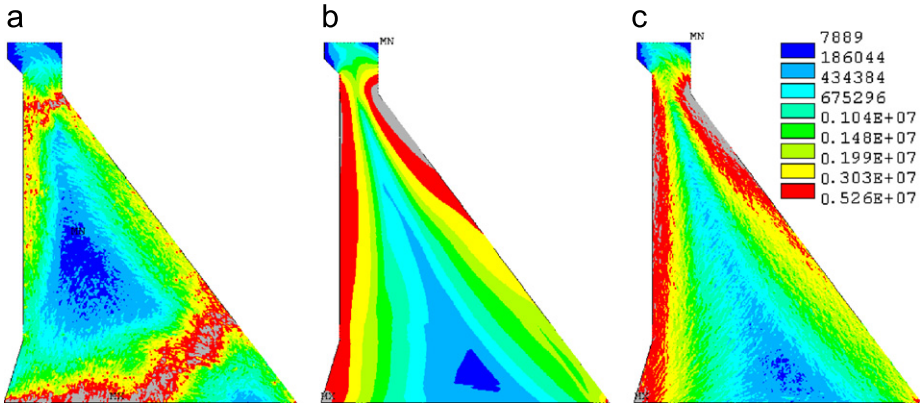

Max: 13.6MPa (Model I) 28.4MPa (Model II) 26.4MPa (Model III)

Fig. 17. Maximum tensile stress of the dam over the seismic range.

stress resembles. In Fig. 17(b), the contour for the homogeneous case is smooth. While from Fig. 17(c) it is quite clear that the stress is not continuous, instead, elements of low stress exist in areas characterized by high stress and vice versa.

From Fig. 17(a) and (c), the effect of nonlinearity can be obtained. In Fig. 17(a), high tensile stress is also observed on the downstream face and upstream face including the dam heel and region with inclination abrupt changes, as in Fig. 17(c). But with the initiation and propagation of cracks, the crack tip is always characterized by high tensile stress, so the stress level along the crack path is generally the highest. In the meantime, owing to stress redistribution caused by cracking, the stress in elements away from the crack is alleviated to some degree.

The acceleration and displacement in the horizontal direction of the dam crest in the first five seconds are plotted in Figs. 18 and 19. Before 1.2 s, the curves of the three models are coincident with each other. Then crack appears and the curve for Model I deviates from the others. Since the presence of crack increases the flexibility of the dam, the period of the dam is elongated, which can be verified by a wider range of wave crests and wave troughs for curves of Model I in the figures. At 2.73 s, cracks on the upstream face and downstream face near the dam neck bridge, and the dam top gets isolated from the dam body. This crack actually acts as a vibration isolation for the dam top, so the vibration of the dam top thereafter is greatly alleviated, as shown in Fig. 18. On the other hand, the isolated dam top leans toward the upstream, as indicated by the negative displacement in Fig. 19. Besides those phenomena, it is worth noting that the acceleration and displacement responses of Models II and III resemble each other in the whole time history, which ensures more realistic simulation of dam response by introducing heterogeneity of concrete yet retaining the overall dynamic property of the dam.

4.6. *Influence of hydrodynamic pressure and unbounded foundation*

Various refined models have been developed to model dam–reservoir interaction and dam–foundation interaction in recent years, other than Westergaard's added mass model and the massless foundation model used in the presented simulation. Since the proposed procedure for seismic damage analysis of concrete dams was formulated in the framework of FEM, it is convenient to be coupled with these refined models to better simulate the influence of the hydrodynamic pressure and unbounded foundation.

In this section, a procedure based on the Scaled Boundary Finite Element Method (SBFEM) [19] is used for modeling the reservoir domain, while the Visco-elastic Boundary Model is used for modeling the unbounded foundation rock, and the results have been compared with those obtained by the aforementioned simpler models in Sections 4.5 and 4.6.

The same material properties for the dam–foundation system and loading condition as in the typical example shown in Fig. 15 are adopted, only that the hydrodynamic pressure and foundation rock are simulated with refined models as have been stated. A comparison of horizontal acceleration time history of the dam crest with that of the typical sample is shown in Fig. 20. Failure pattern of the dam is shown in Fig. 21.

Although more refined modeling of the reservoir and foundation rock has been adopted, the seismic response of the dam, including shape of the curve of acceleration and deformation curve as well as failure process of the dam, is similar to that of simple models. Emphasis will be placed on the analysis of the difference. Owing to the time needed for the wave to propagate from the foundation boundary, a time lag of about 0.06 s in the initial phase of the acceleration time history exists, which

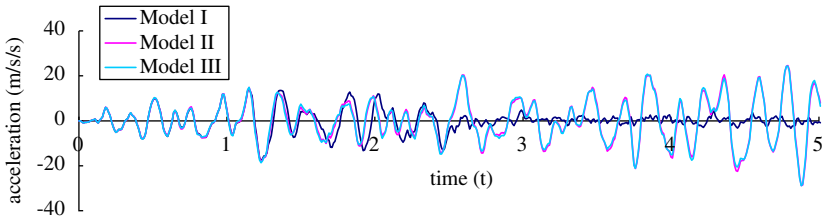

Fig. 18. Horizontal acceleration response of the dam crest.

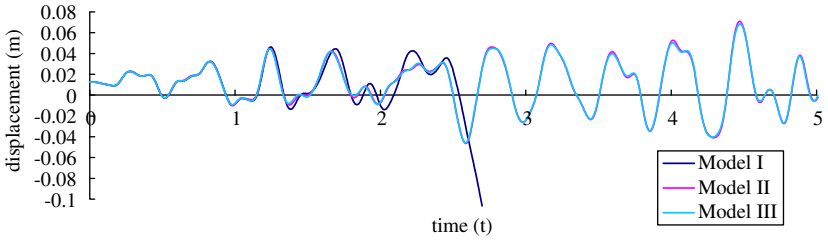

Fig. 19. Horizontal displacement response of the dam crest.

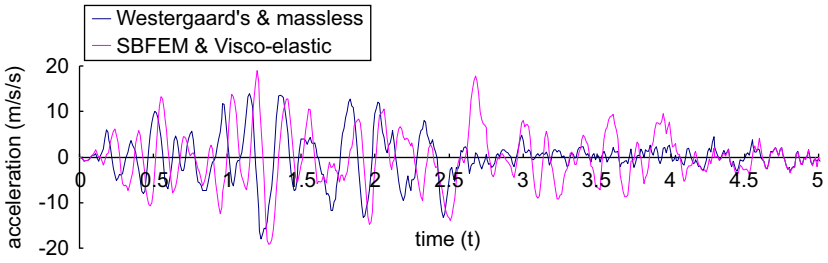

Fig. 20. Horizontal acceleration response of the dam crest.

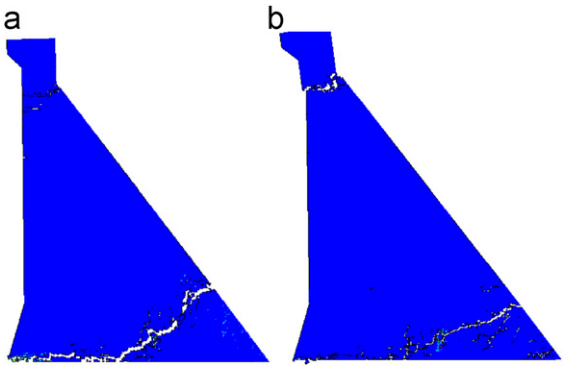

Fig. 21. Failure pattern of the dam. (a) Westergaard's model and massless foundation and (b) SBFEM model and Visco-elastic Boundary Model.

gradually reduces to 0.04 s at about 2 s, indicating a slight change in the natural frequency of the dam owing to consideration of the reservoir. In the case of the refined model, the time for abrupt decrease in acceleration of dam crest occurs later than that of the simple model, indicating late failure of the dam neck. Damage process of the dam is quite similar to that obtained by the simple models. As shown in Fig. 21, cracks at the dam neck and at the lower part of the dam are also observed. The lower crack initiates at the dam heel, propagates for a similar distance almost horizontally and kinks into the dam body by a smaller angle.

It can be said that Westergaard's added mass model and massless foundation are adequate to the model effect of reservoir and foundation rock in Section 4.4.

5. Conclusion

Tang's RFPA is extended to seismic failure analysis of concrete dams and new perspectives regarding seismic failure of gravity dams are obtained. Small finite elements are used for discretization of the dam and influence of heterogeneity of concrete is approximated by random distribution of material properties. Solution of equation of motion by α-Newmark algorithm combined with improved SSOR-PCG guarantees stable and efficient solution to this strong nonlinear and computational intensive problem. When compared with existing models for dynamic nonlinear analysis of concrete dams, the proposed approach has the advantage that no information on cracking route is needed beforehand, no remeshing at crack tip is required and initiation and propagation of cracks can be achieved automatically according to response of the dam. In addition, this procedure can be applied to dynamic failure modeling of other large scale concrete structures.

Taking a practical gravity dam as an example, typical failure process and failure modes of gravity dams are studied. Damage and cracking of gravity dams in earthquakes are caused mainly by excessive tensile stress. When heterogeneity of concrete is considered, stress distribution is not smooth any more, which better reflects the real situation. Quite a few small cracks may occur in regions with a high-stress level, including dam neck, dam faces, dam heel and so on. A few of them propagate, bridge, coalesce and evolve into dominant cracks, while others remain stable until shocking ends. Relatively smaller earthquake may cause damage to the dam neck while a bigger one may bring on cracks at lower parts of the dam. Cracking at the dam neck, dam bottom and abrupt change in slope of dam face are most often observed. Cracking at the dam bottom does not all along follow a horizontal route, instead, it inclines to a direction almost perpendicular to the downstream face.

The present research serves as an exploration of numerical simulation of seismic failure process of large scale engineering concrete structures such as high dams considering the influence of heterogeneity of concrete. Certain aspects, including thresholds in the constitutive relations and reasonable consideration of concrete heterogeneity in analysis of big bulk concrete structures, merit further investigation and validation, probably by comparison with experiments. With the on-going of this research, these aspects will be clarified gradually.

Acknowledgment

Financial supports from the National Nature Science Foundation of China (90510018, 90915009 and 51009019) as well as Fundamental Research Funds for the Central Universities are greatly acknowledged. In addition, the authors wish to thank Prof. C.A. Tang and Associate Prof. Z.Z. Liang for their enlightening suggestions. The help from Dr. C.G. Zhou and Y. Wang on refining the computation is also acknowledged.

References

[1] Standard of Ministry of Electric Power, PRC. Specifications for Seismic Design of Hydraulic Structures (DL 5073-2000). Beijing: China Electric Power Press; 2001.
[2] Lin G. Performance of dams suffered in Wenchuan earthquake and seismic safety analysis of dams. Journal of Dalian University of Technology 2009; 49(5):657–66 [in Chinese].
[3] Li QS, Li ZN, Li GQ, et al. Experimental and numerical seismic investigations of the Three Gorges dam. Engineering Structures 2005;27(4):501–13.
[4] Harris DW, Snorteland N, Dolen T, Travers F. Shaking table 2-D models of a concrete gravity dam. Earthquake Engineering and Structural Dynamics 2000;29:769–87.
[5] Lotfi V, Espandar R. Seismic analysis of concrete arch dams by combined discrete crack and non-orthogonal smeared crack technique. Engineering Structures 2004;26:27–37.
[6] Mirzabozorg H, Ghaemian M. Non-linear behavior of mass concrete in three-dimensional problems using a smeared crack approach. Earthquake Engineering and Structural Dynamics 2005;34(3):247–69.
[7] Calayir Y, Karaton M. A continuum damage concrete model for earthquake analysis of concrete gravity dam–reservoir systems. Soil Dynamics and Earthquake Engineering 2005;25(11):857–69.
[8] Kuhla E, Ramm E, de Borst R. An anisotropic gradient damage model for quasi-brittle materials. Computer Methods in Applied Mechanics and Engineering 2000;183(1–2):87–103.
[9] Valliappan S, Yazdchi M, Khalili N. Earthquake analysis of gravity dams based on damage mechanics concept. International Journal for Numerical and Analytical Methods in Geomechanics 1996;20(10):725–51.
[10] Horii H, Chen S. Computational fracture analysis of concrete gravity dams by crack-embedded elements—toward an engineering evaluation of seismic safety. Engineering Fracture Mechanics 2003;70(7–8):1029–45.
[11] Pekau OA, Cui Y. Failure analysis of fractured dams during earthquakes by DEM. Engineering Structures 2004;26(10):1483–502.
[12] Lin G, Wang J, Hu Z, Liu J. On the dynamic stability of potential sliding mass during earthquakes. In: Proceedings of the fifth international conference on dam engineering. Lisbon, Portugal; 2007.
[13] Hou Y, Zhang C, Cui Y. Study on seismic damage and rupture of arch dams by rigid-spring elements. Journal of Hydroelectric Engineering 2004;23(4). 20–25, 30 [in Chinese].
[14] Zhu W, Tang C. Numerical simulation on shear fracture process of concrete using mesoscopic mechanical model. Construction and Building Materials 2002;16(8):453–63.
[15] Tang CA, Kou SQ. Crack propagation and coalescence in brittle materials. Engineering Fracture Mechanics 1998;61(3/4).
[16] Miranda I, Ferencz RM, Hughes TJR. An improved implicit–explicit time integration method for structural dynamics. Earthquake Engineering and Structural Dynamics 1989;18(5):643–53.
[17] Lin S. Improved iteration format of symmetric successive over relaxation—preconditioned conjugated gradient method. Journal of Numerical Methods and Computer Applications 1997;4:266–70 [in Chinese].
[18] Zhong H. Large-scale numerical simulation for damage prediction of high arch dams subjected to earthquake shocks. PhD thesis, Dalian University of Technology, China; 2008 [in Chinese].
[19] Wang Y, Lin G, Hu Z. Coupled FE and Scaled Boundary FE—approach for the earthquake response analysis of arch dam–reservoir–foundation system. In: Proceedings of the ninth world conference on computational mechanics. Sydney, Australia; 2010.